

## Article

# Microrheology to Understand the Viscosity Behavior of a Sophorolipid Biosurfactant

Jochen Kleinen, Jan Langwald, Joachim Venzmer and Hacer Yalcinkaya \*

Evonik Operations GmbH, Research Interfacial Technology, Goldschmidtstr. 100, 45127 Essen, Germany; jochen.kleinen@evonik.com (J.K.); jan.langwald@evonik.com (J.L.); joachim.venzmer@evonik.com (J.V.)  
\* Correspondence: hacer.yalcinkaya@evonik.com

**Abstract:** The microstructure of the aqueous solutions of purified acidic Sophorolipid (SL) has previously been studied using highly sophisticated methods such as SANS and Cryo-TEM. We were interested in whether (a) the main findings also apply to commercially available SL (which is a mixture of acidic and lactonic SL) and (b) more readily available methods such as DLS can be used to gain insight into the molecular aggregation of SL. Our work was motivated by the increasing interest in biosurfactants for applications in personal and household care. Moreover, the origin behind the more or less lack of rheological response to changes in pH is of practical relevance, as it is somewhat unusual for a carboxylate-group containing surfactant. By using DLS microrheology, we could elucidate the aggregation structure and dynamics of the surfactant on a microscopic scale. Surprisingly, the different degrees of protonation only impacted the microscopic properties such as exchange kinetics and the plateau values of the storage moduli.

**Keywords:** sophorolipid; microrheology; dynamic light scattering; viscoelasticity



**Citation:** Kleinen, J.; Langwald, J.; Venzmer, J.; Yalcinkaya, H. Microrheology to Understand the Viscosity Behavior of a Sophorolipid Biosurfactant. *Colloids Interfaces* **2022**, *6*, 3. <https://doi.org/10.3390/colloids6010003>

Academic Editor: Jaroslav Katona

Received: 26 November 2021

Accepted: 30 December 2021

Published: 4 January 2022

**Publisher's Note:** MDPI stays neutral with regard to jurisdictional claims in published maps and institutional affiliations.



**Copyright:** © 2022 by the authors. Licensee MDPI, Basel, Switzerland. This article is an open access article distributed under the terms and conditions of the Creative Commons Attribution (CC BY) license (<https://creativecommons.org/licenses/by/4.0/>).

## 1. Introduction

Biosurfactants are surface-active materials produced by microorganisms. They have attracted much interest in recent years due to advantages such as biodegradability, non-toxicity and compatibility with biological materials (mildness towards enzymes and skin) [1–4]. One of the best known biosurfactants is Sophorolipid (SL), which is basically a glycolipid consisting of a sugar and a lipid moiety that are covalently linked. As an amphiphilic molecule, various beneficial properties have been reported, such as remarkable surface activity, dispersing and foaming [5–7]. Hence, it is being increasingly used in cosmetic, food, medical and detergency applications [1,8,9].

The mixture of lactone (the fatty acid moiety forms a closed lactone ring) and acidic SL (the fatty acid has a free carboxylic acid end) (see Supplementary Information Figure S1) reveals a synergism leading to improved performance in interfacial activities [6]. In the work of Hirata et al., the surface tension and detergency of acidic and lactonic SLs were tested separately and at different mixing ratios. In the end, the mixture showed a better improvement in terms of all physicochemical properties; moreover, it was found that the foam properties could be controlled by the ratio between two SL types [6,9]. Additionally, it was shown before that the acidic form plays a role in increasing solubility and foamability, while the lactone form has a significant effect on antimicrobial activity [10,11]. Moreover, SL might serve as a platform for surfactants of the next generation, as several derivatives have been reported and all the different types (including bola form) behave distinctly different [12,13].

Usually, the aggregation behavior of surfactants can be predicted by using the Critical Packing Parameter concept conceived by Israelachvili [14]. In the case of SL, the peculiar bola architecture precludes the straight-forward application of this concept, as has been shown recently in more detail by Baccile et al. [15].

In previous works, particularly the isolated acidic form of SL has been studied in terms of its interesting self-assembly behavior as a function of pH or temperature [16,17]. At lower pH as a function of concentration, SL forms spherical or rod-like micelles. It was reported for the acidic SL that the free COOH group enables a stimuli-responsive behavior. The degree of ionization of the COOH group changes with pH leading to sphere-to-rod or rod-to-sphere transitions even at very low SL concentrations [17].

We have seen that solutions of the commercially available acidic/lactone SL mixture do not show explicit viscoelastic behavior at different pH values. This is somewhat surprising, since other surfactants containing carboxylate groups, such as fatty acids (i.e., soaps), amino acid surfactants or rhamnolipids exhibit significant changes in phase and aggregation behavior at different pH values, leading to noticeable changes in flow behavior [18–20]. Rhamnolipids, another increasingly popular type of biosurfactants, form lamellar structures at a low pH, which upon an increase in pH convert into vesicles and for even higher pH values into micelles [21]. As a consequence, the viscosity of rhamnolipid solutions drastically changes with pH value.

One option to build viscosity in surfactant formulations is to utilize the interaction between surfactants and co-surfactants, which is of major interest for applications in both home care and personal care. A prominent example is the synergy between sodium lauryl ether sulfate (SLES) and cocamidopropyl betaine (CAPB) at low pH [22,23]. Amin et al. studied the distinct influence of rhamnolipid on the rheological behavior of formulations containing SLES and CAPB [22]. Rheologically speaking, viscosity is generated mainly by the two following properties of the surfactant aggregates formed: the crosslink density of the micelles and their average lifetimes. In contrast to spherical micelles, worm-like micelles can entangle and form crosslinks. Thus, influencing the conditions under which distinct surfactant aggregates form is of great relevance; the kinetics of micelle formation and of the surfactants at interfaces are dynamic processes which are of importance for many applications [24].

The rheological parameters crosslink density and exchange kinetics can be derived using the Maxwell model; a detailed introduction and description can be found elsewhere [25]. Storage modulus  $G'$ , loss modulus  $G''$  and structural relaxation time  $\tau$  are usually being obtained by mechanical rheometry, since the wormlike micelles present in standard surfactant formulations are sufficiently long and long-living to be studied by mechanical oscillatory rheology. The attainable frequency range is, however, limited by the inertia of the measuring geometry to about 10 rad/s for viscosities below 1000 mPas [26]. Therefore, in case samples of low viscosity, when fast dynamics need to be investigated, microrheology, based on Dynamic Light Scattering (DLS), has been employed [27]. Classically, DLS measures the diffusion/displacement of scattering objects in a sample of known viscosity to quantify their size via the Stokes-Einstein equation. By measuring the displacement of particles of known size, the viscosity (and other rheological parameters) can be determined. The tracer particles need to be added in such a concentration that the scattered light is dominated by the particles. Their movement through the thermal fluctuations in the sample allow for the obtention of the viscoelastic information of the sample indirectly from the Stokes-Einstein equation [28].

Different viscoelastic systems have already been intensively studied using DLS microrheology. Among them are surfactant solutions, complex polymer hydrogels and biological materials [29–31]. In the work of Xu and Amin, the rheological effect of rhamnolipid on the abovementioned mixed surfactant system was studied using traditional rheology coupled with microrheology for the higher frequency regime [22]. Thus, the viscoelastic response to different formulation conditions such as salt and pH could be screened. In another study, microrheology was used effectively to determine the rheology of industrially relevant protein solutions and the viscoelastic behavior of their temperature-dependent aggregation [32].

In our study, we have examined the micellar aggregation behavior of a commercially available version of SL, which consists of a mixture of acidic and lactonic forms, by using

straightforward and easily applicable rheological methods. The motivations behind our work were the following questions: (a) Does a commercially available SL mixture behave in principle like the highly purified samples of acidic SL investigated by SANS and electron microscopy? [15–17,33]; (b) Can DLS microrheology be used to obtain a better understanding of the fundamental micellar parameters of SL and their dynamics? This information will be helpful to understand the comparably limited responsiveness of the viscosity to changes in the pH value as well as how to develop formulations having appropriate viscosities.

## 2. Materials and Methods

**Materials:** Sophorolipid (SL) used in this work is a mixture consisting of 60% acid and 40% lactone and is available as REWOFERM® SL ONE by Evonik Operations GmbH, Essen, Germany. The active content is 40%; the pH value is 5.8.

**Sample Preparation:** Samples were prepared in 50 mL volume and diluted with Millipore water to the desired concentrations. Subsequently, the pH values were adjusted with 30% citric acid and 30% KOH for all samples. Minimal addition of acid or base was needed for the highest dilutions of 5% and 10% to compensate the small changes in pH upon dilution. Concentrations are given as active matter SL (in percent).

**Dynamic Light Scattering (DLS):** Measurements were performed with a Zetasizer Nano ZS (Malvern Instrument Lab, Malvern, UK) equipped with a 4 mW He-Ne laser with a wavelength of 633 nm. Samples were filtered using a 0.45 µm filter prior to the measurements. Each measurement was repeated three times and the results are averaged. In this method, scattered light is detected in a specific time frame to monitor the particle movements. Depending on the particle size, scattered light intensity shows different fluctuations. The autocorrelation function curves represent these intensities and reveal how long a particle is present at the same location in the sample. While small particles can move faster, the time they need to change their position is shorter. This reflects as a faster decay on the autocorrelation function curve. Conversely, for larger particles, the decay is delayed due to their rather slow movement. Particle sizes were obtained from the autocorrelation functions measured by the instrument; the size distributions were determined via the cumulant method, which is implemented in the Malvern software.

**DLS microrheology:** The mean square displacement (MSD) of tracer particles is measured by DLS; the data is compiled by a generalized Stokes-Einstein relationship to obtain viscoelastic parameters [34]. The tracer particles are added in such a concentration that the scattering intensity of the particle dominates the sample by a factor of at least 100; this was realized by adding 6 µL of 200 nm particles (Sigma-Aldrich Chemie GmbH, Steinheim, Germany, micro particle size standard based on polystyrene monodisperse 0.2 µm size; 2% solid content) to 1.2 mL of the sample. After the addition of the particles, the samples were vortexed for 30 s and then placed in an ultrasonic bath for 1 min to remove air bubbles. Each sample has been measured three times and the values obtained (cross-over frequency and plateau value) agreed within 10%.

A feature key of the Malvern Software is needed in order to perform microrheology with the Zetasizer Nano ZS [35]. A detailed description of the method can be found elsewhere [32]. The applicability to surfactant systems has already been discussed in more detail [28]. Microrheology provides insights into the fast dynamics of samples, whereas the behavior on a seconds, minutes and hours scale is usually probed by mechanical rheology [36].

**Oscillatory Shear Rheology:** Mechanical rheology was performed on an AR-G2 Rheometer (TA Instruments, Eschborn, Germany) using a 25 mm parallel plate geometry. The temperature was controlled by a Peltier device in the lower plate; the gap was set to 0.25 mm. Worm-like surfactant micelles can well be described by the Maxwell model; the crossover frequency that gives information on the dynamics of micelles deeply depends on the structure of the surfactant and influences (together with the network density of the micelles) the viscosity of the sample. Both parameters, i.e., crossover frequency and network density, can be obtained by oscillatory rheological measurements, if the accessibility was

given [37]. Any mechanical rheometer is limited by the inertia which limits the upper end of the frequencies that can be probed, [38] even though today's rheometers have excellent sensitivity in terms of torque [39].

The parameters obtained from both rheological methods can be listed as: Crossover: The frequency at which the storage modulus becomes larger than the loss modulus when going from low frequencies to high frequencies given in rad/s (see Figure 3a; the crossover of moduli is not exactly right since some plots have two crossovers).  $G^0$  (spectra): The maximum value of the storage modulus  $G'$  at high frequencies; the plateau value is given in Pa.  $G^0$  (cole-cole): The plateau value  $G^0$  equals twice the value of the storage modulus at the crossover frequency; the moduli at the crossover frequency are equal (and the loss modulus is at its maximum), so the value of the moduli at crossover can be easily extracted from the cole-cole plots (see Supporting Information). Duplicating this value then gives the plateau value  $G^0$  (cole-cole) in Pa. Zero shear viscosity from microrheology: This viscosity can be calculated by dividing  $G^0$  (spectra) by the crossover frequency (compare the Cox-Merz rule [40]). Viscosity from mechanical measurement: The mechanical measurements of the frequency spectra yield the complex viscosity; the values at low frequencies were used (Cox-Merz rule).

### 3. Results and Discussion

The submicron structures formed by SL are strongly dependent on pH and concentration [16,17,41]. In this regard, we have examined the viscoelastic behavior of different SL concentrations between 5–40% ( $w/w$ ) at pH 3 and pH 8. These pH values of 3 and 8 were chosen, since this covers the range from fully protonated (pH 3) to fully deprotonated (pH 8), considering the pKa of 5.8–6.1 [17,42]. Subsequently, the impact of temperature on these microstructures is investigated.

In Figure 1, the correlation functions from DLS measurements for the increasing concentrations of SL at pH 3 (Figure 1 left) and pH 8 (Figure 1 right) are presented. Comparing the plots on the left and right sides at a first glance, the difference among the relaxation times is clearly visible. This can be interpreted as follows: For samples up to 30% SL at pH 8, the particle size is smaller than for the corresponding solutions at pH 3. The correlation functions for samples at pH 3, as explained in the methods section, shift from a fast monomodal decay to a slow bimodal behavior along with the concentration increase. This means the particle size increases with increasing concentration. At pH 8, fast monomodal decay behavior almost stagnates for concentrations up to 30%, indicating a very small size growth. For 30 and 40% ( $w/w$ ) samples, a second mode appears for pH 8, reflecting the increased polydispersity of the particles (see Table S1 in Supplementary Information).

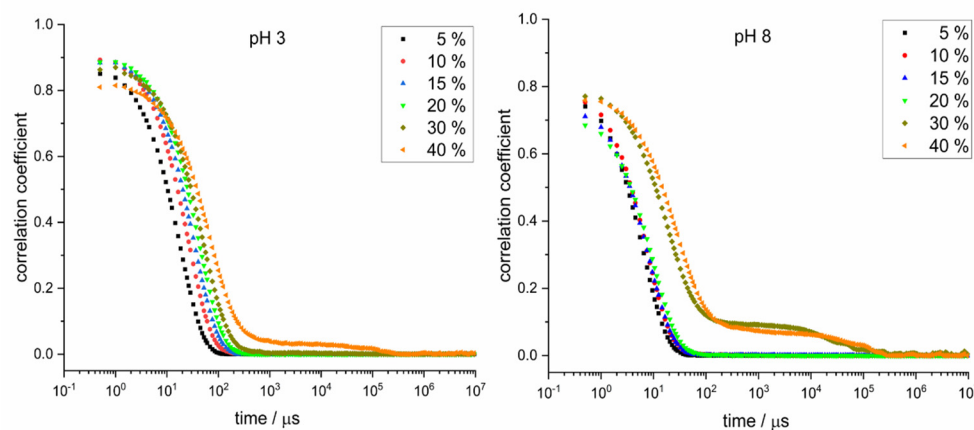


**Figure 1.** Correlograms of Sophorolipid (SL) in water at different concentrations (mass %) at left) pH 3 right) pH 8.

Such a growth in the size and size distribution of micelles typically causes a distinct effect on viscosity. Therefore, a deeper look into the viscoelastic properties of the samples using DLS microrheology allowed us to understand the molecular evolution of the aggregates. The trend that the lifetimes of the worm-like micelles shift to longer timescales with increasing concentration can also be seen in the frequency-dependent measurements of microrheology (Figure 2). The data shift to lower frequencies (i.e., longer time scales) with increasing concentration. All the measurements show a Maxwell behavior, meaning that the storage modulus  $G'$  scales with a slope of 2, whereas the loss modulus  $G''$  scales with a slope of 1. The scaling of the data as a function of frequency according to the Maxwell model can also be seen from the Cole-Cole plots (see Supplementary Information Figures S3 and S4). These plots show (parts of) semi-circles; the height of the semi-circle is equal to the moduli at the crossover frequency. Figure 2 only shows the measurements of the concentrations from which rheological parameters could be extracted (see Table 1); additional data on samples containing 5% and 10% SL can be found in the Supplementary Information (Figure S2 left and right).

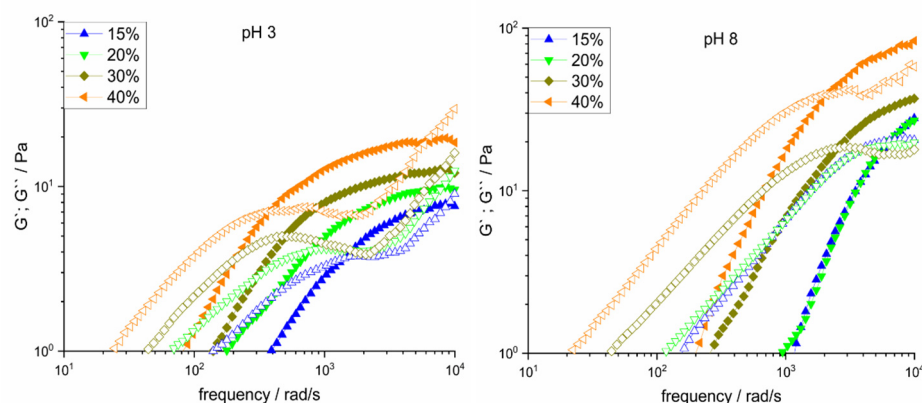


**Figure 2.** Evolution of the frequency response of  $G'$  (filled),  $G''$  (open symbols) of Sophorolipid (SL) in water at different concentrations (mass %) at left) pH 3 right) pH 8.

**Table 1.** Summary of the parameters obtained from (micro-)rheology measurements for different SL concentrations at pH 3 and pH 8.

Concentration/%	Cross-over/rad/s	$G^0$ (spectra)/Pa	$G^0$ (cole-cole)/Pa	Calculated	Mechanical
				Zero shear viscosity from microrheology/mPas	Viscosity from mechanical/mPas
<b>pH 3</b>					
15	1430	7.7	7.3	5.4	-
20	780	9.6	10	12	7.2
30	500	12	12	24	16
40	380	19	16	50	42
<b>pH 8</b>					
15	6390	41	41	6.0	4.1
20	5800	35	40	6.0	4.8
30	2500	39	47	16	12
40	2070	92	80	44	63

For a detailed explanation of the listed parameters, see the materials and methods section.

The frequency at which the crossover of both moduli occurs also depends on the concentration of the samples, as can also be seen from Figure 2. The crossover frequency is a timescale which can be used as an indicator for the average lifetime of a surfactant aggregate. Following the measured data to higher frequencies shows a leveling of the storage modulus  $G'$ . This plateau value  $G^0$  is a measure of the crosslink density (entanglements) of the surfactant aggregates; the plateau value  $G^0$  equals twice the storage modulus at the crossover frequency [25]. Both the crossover frequency and the plateau value influence the

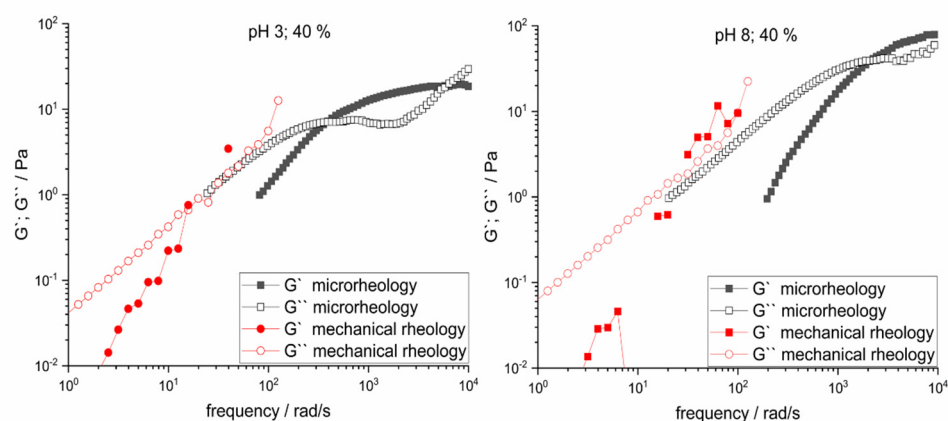
viscosity of the surfactant system; control of these parameters allows for the tuning of the viscosity of surfactant formulations. Comparing the data at pH 3 and pH 8 shows that the crossover frequencies at pH 3 are lower than those at pH 8; however, the plateau value  $G^0$  for the pH 3 samples are also lower than the ones at pH 8. The general shape of the mechanical spectra does not change but follows the modified Maxwell model (compare also the Cole-Cole plots in Figures S3 and S4 in the Supplementary Information) [43]. The different pH values (i.e., the state of protonation) lead to a shift of the curve in terms of both frequencies and moduli. The samples at 5% and 10% active matter could be measured but did not show a Maxwell-type behavior anymore due to the shifting of the curves to higher frequencies. Thus, rheological parameters could not be extracted for these two samples.

Table 1 shows that the values of the crossover frequencies of the moduli (equivalent to relaxation times in the millisecond range) at high pH values are higher by about a factor of 5.

The plateau value of the storage modulus can be determined in different ways: One option is to double the value of the storage modulus at the crossover frequency, which is described by  $G^0$ ; the other option is to examine the Cole-Cole plots and draw/complete (manually) the semi-circle and multiply the value at the maximum of the semi-circle by two. The second method was done manually and is prone to have minor errors; however, both values match quite well.

The viscosity at low shear rates can be computed from the crossover frequency/typical time scale and the plateau value of the storage modulus. Although the parameters develop differently for SL at the two different pH values, the product of the two parameters yields similar viscosities of around 45–50 mPas for the 40% solutions. The viscosity of these two samples have also been measured by using a mechanical rheometer, giving similar results. One might ask the question why we took the effort to measure the viscosity by microrheology and not by using a standard rheometer. By the extension of the frequency range in microrheology, we could see why the macroscopic viscosity was more or less independent of pH. At different degrees of protonation, the effects of changes in the lifetime and crosslink density of the micelles cancel each other out.

We have used our mechanical rheometer to perform oscillatory rheology in order to see whether these moduli compare well with the data obtained by DLS microrheology. Figure 3 shows the combination of the mechanical and the microrheological spectra for the two pH values at their highest concentrations. Especially the loss moduli  $G''$  show no perfect scaling but some deviation at frequencies above 10 rad/s [26,27]. The continuation of the loss moduli matches well with the ones obtained by microrheology measurements, although it has been reported that perfect overlays of the two methods are hard to achieve [44]. The storage moduli  $G'$  obtained by mechanical rheology shows a scaling by a factor of 1, which is expected if the samples respond according to the Maxwell model. The crossover of storage and loss moduli are, however, at too low frequencies, which would not correspond to the low viscosity (a shift of a factor of 10 in the crossover frequency would also lead to a difference in viscosity by that factor). The shift of the storage modulus to higher values is attributed to inertia effects. These effects depend on the gap size, and the measured values of the storage modulus approach the true value with lowering the gap size of the rheometer [45]. This will, however, only give an approximation of the true value and furthermore may not allow for measurement at high frequencies to resolve the true crossover frequencies and plateau values. The evolution of moduli at higher frequencies develops differently, however, indicating a change in structure of the micelles at the two pH values, as discussed above. The complex viscosity that can be derived from the measurements shown in Figure 3 are presented in the Supporting Information (Figures S5 and S6).



**Figure 3.** Combination of classical rheology and microrheology illustrating the evolution of the frequency response of  $G'$  (filled),  $G''$  (open symbols) of Sophorolipid (SL) in water at 40% concentration ( $w/w$  %) at left) pH 3 right) pH 8.

The structure of the micelles at the two pH values was also probed by another series of measurements at different temperatures. The concentration of SL was kept constant at 40%, and the measurement at 25 °C was used to check for reproducibility of the measurements. The results are shown in Figure 4 and summarized in Table 2. It is obvious that the data points develop differently depending on the temperature for the two states of protonation. The moduli for SL at low pH shift to lower values, while the position of the crossover frequency hardly changes and stays more or less constant between 200–300 rad/s. The crossover frequencies at pH 8, however, shift to higher frequencies with increasing temperature, while the level of the moduli stays constant at around 90 Pa. This shift of the spectra with temperature to different frequencies while the moduli stay constant can also be seen if the data are plotted as Cole-Cole plots (see Supplementary Information, SI Figures S7 and S8). All five semicircles coincide for the measurements of the pH 8 sample, while the shift of the samples at pH 3 can be recognized on account of the semicircles having different diameters.

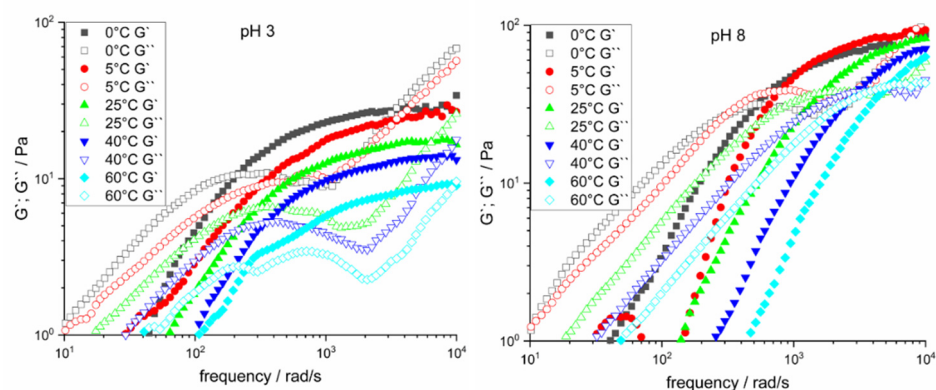


**Figure 4.** Evolution of the frequency response of  $G'$  (filled),  $G''$  (open symbols) for 40% concentration ( $w/w$  %) Sophorolipid (SL) in water at different temperatures at left) pH 3 right) pH 8.

**Table 2.** Summary of the parameters obtained from (micro-)rheology measurements for 40% SL concentration at different temperatures at pH 3 and pH 8.

Temperature/°C	Cross-over/rad/s	G <sup>0</sup> (spectra)/Pa	G <sup>0</sup> (cole-cole)/Pa	Calculated	Mechanical
				Zero shear viscosity from mi- corrheology/mPas	Viscosity from mechani- cal/mPas
<b>pH 8</b>					
0	515	72	66	140	200
5	780	90	91	115	150
25	1571	94	96	60	60
40	2870	84	80	30	33
60	5300	90	115	17	17
<b>pH 3</b>					
0	215	28	26	130	140
5	325	25	24	77	70
25	300	18	14	60	42
40	360	13	12	36	30
60	240	9	8	38	22

For a detailed explanation of the listed parameters, see the materials and methods section.

Rheological measurements performed at the different temperatures may be combined to one curve (master curve). The measurement at 25 °C was taken as a reference. Master curves are usually obtained in order to enlarge the accessible frequency range of (molten) polymers; a sample is measured at different temperatures in a specified range of frequencies. One (usually) higher temperature is taken as a reference temperature; the measurements at lower temperatures obtained in the same frequency range behave like the polymer at the higher temperature; the behavior is, however, shifted to longer timescales and the frequency range can be enlarged by superposition/shifting of the obtained spectra. The micelles of SL could in principle be measured at lower temperatures by mechanical rheology, and the results could be shifted to the reference temperature (of, e.g., 25 °C) in order to enlarge the accessible frequency range of the mechanical rheometer. The window for measurements in aqueous systems is, however, limited to about 80 °C; temperatures below 0 °C might lead to freezing of the sample, whereas evaporation would cause wrong results at high temperatures. Additionally, the structure of the surfactant aggregates may change with temperature, which would make a scaling impossible.

Figure 5 shows the master curves (dynamic rheological spectra at different temperatures) of SL at low and high degrees of deprotonation. The formation of the master curve failed for the sample at a low pH value, whereas the curves could be matched at high pH values. This result furthermore proves that SL forms different aggregates at different pH values (degrees of protonation); the structures of the aggregates formed at low pH values are influenced by temperature, presumably because hydrogen bonds play an essential role in the structures formed by the biosurfactant, whereas the influence of temperature and thus the impact of hydrogen bonds are negligible at high pH values. The SL is charged at high pH values and the deprotonated carboxylic acid groups are not able to interact via hydrogen bonds with other groups such as the sugar groups anymore. Baccile et al., e.g., followed inter- and intramolecular H-bonds on purified SL acid at different pH values by NMR [17,46]. Thus, the degree of protonation deeply influences the type of aggregation, explaining the differences in the microscopic behavior.

Interestingly, the viscosity obtained from microrheology measurements (crossover frequency and plateau moduli) are again in about the same order of magnitude for the two different pH values and start around 130 mPas at 0 °C and drop to 20–30 mPas at 60 °C. The measurement at 25 °C gave viscosities of 60 mPas which is perfectly in line with the mechanical measurement (compare Table 1). The insights into the behavior of the SL at different pH values by microrheology are helpful to understand why the viscosity of the surfactant samples, which is a macroscopic effect, is quite similar at pH 3 and at pH 8. Coincidentally, the effects of the different microscopic parameters (i.e., plateau modulus and crossover frequency) cancel each other out to yield a similar macroscopic property.

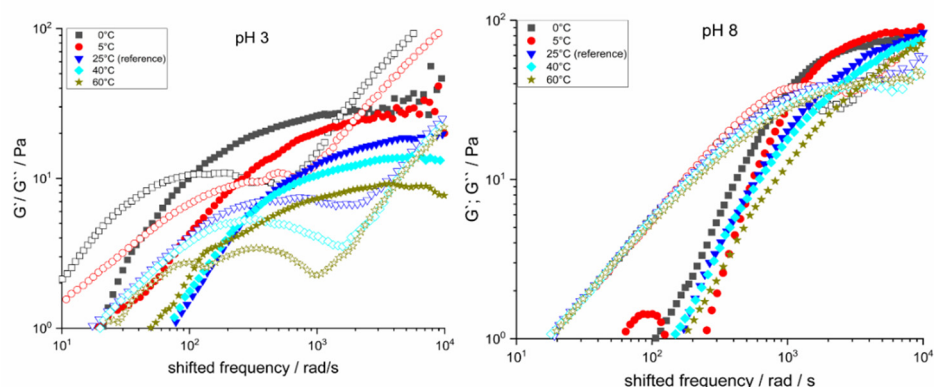


**Figure 5.** Master curves, dynamic rheological spectra of 40% concentration ( $w/w$  %) of Sophorolipid (SL) at different temperatures at left) pH 3 right) pH 8,  $G'$  (filled),  $G''$  (open symbols).

#### 4. Conclusions

We have studied the aggregation behavior of commercial SL as a mixture of both lactone and acidic forms. Interestingly, SL aggregates do not show a pronounced change in viscosity as a function of concentration and pH, although the acidic form contains a carboxylic acid moiety. The different degrees of protonation do not lead to a drastic change in the aggregation behavior typical of soaps; here, rather, the effects happen on a microscopic scale. Therefore, a deeper rheological characterization could provide insights into the exchange kinetics of these aggregates. Despite the use of standard industrial equipment, the general trends depending on concentration and temperature could be derived. Recently, the DLS microrheology method has even been further improved [31].

The exchange kinetics of SL are comparably fast, although they carry a long hydrophobic chain, for which one would expect a lower crossover frequency [22,37]. The unusual behavior of SL is attributed to the double hydrophilic (bola) structure of the molecule, carrying both a sugar group and a carboxylic acid group on each side of the hydrophobic part. Thus, it is not too surprising that attempts to describe the molecule by the concept of critical packing parameter somewhat failed [15]. We could show by microrheology measurements that the structure and the dynamics of the surfactant change with pH value and temperature on a microscopic scale. The changes on a microscopic scale are, however, not that obvious by considering macroscopic parameters like consumer-perceived viscosity, which is in contrast to other pH-sensitive surfactants. Also, Baccile et al. saw a similar change in behavior, namely, the increase in surface charge on SL micelles, which was probed on a microscopic scale by SANS [47]. Furthermore, the time-dependent effects of protonation have been reported for worm-like micelles, which can lead to different kinetic behavior/structure and thus viscosity/rheology [48]. These changes can be followed by macroscopic methods; in the case of the SL, however, the changes could only be detected by microscopic parameters. Our investigations further help to understand the complex behavior of SL, which is an interesting class of biosurfactants since their behavior can be tuned by derivatization from highly dynamic to “frozen” type bola-SL [9].

**Supplementary Materials:** The following are available online at <https://www.mdpi.com/article/10.3390/colloids6010003/s1>, Figure S1: Chemical structures of different SL types; Figure S2: Evolution of the frequency response of  $G'$  and  $G''$  of SL at different concentrations at left) pH 3 right) pH 8; Figure S3: Cole-Cole plots of SL at pH 3 (different concentrations); Figure S4: Cole-Cole plots of SL at pH 8 (different concentrations); Figure S5: complex viscosity of 40% SL pH 3; Figure S6: complex viscosity of 40% SL pH 8; Figure S7: Cole-Cole plots of SL at pH 3 (different temperatures); Figure S8: Cole-Cole plots of SL at pH 8 (different temperatures); Table S1: Particle size and PDI of SL from DLS.

**Author Contributions:** Conceptualization, J.K. and H.Y.; Formal analysis, J.K., J.L. and H.Y.; Investigation, J.L.; Visualization, J.K. and H.Y.; Writing—original draft, J.K. and H.Y.; Writing—review & editing, J.V. All authors have read and agreed to the published version of the manuscript.

**Funding:** This research received no external funding.

**Institutional Review Board Statement:** Not applicable.

**Informed Consent Statement:** Not applicable.

**Data Availability Statement:** Not applicable.

**Acknowledgments:** The authors would like to thank Stefanie Volkmer for sample preparation.

**Conflicts of Interest:** The authors declare no conflict of interest.

**Sample Availability:** Samples of the compounds are not available from the authors.

## References

1. Roy, A. A Review on the Biosurfactants: Properties, Types and its Applications. *J. Fundam. Renew. Energy Appl.* **2018**, *8*, 1–5. [[CrossRef](#)]
2. Akbari, S.; Abdurahman, N.H.; Yunus, R.M.; Fayaz, F.; Alara, O.R. Biosurfactants—a new frontier for social and environmental safety: A mini review. *Biotechnol. Res. Innov.* **2018**, *2*, 81–90. [[CrossRef](#)]
3. Adu, S.A.; Naughton, P.J.; Marchant, R.; Banat, I.M. Microbial biosurfactants in cosmetic and personal skincare pharmaceutical formulations. *Pharmaceutics* **2020**, *12*, 1099. [[CrossRef](#)]
4. Dierickx, S.; Castelein, M.; Remmery, J.; De Clercq, V.; Lodens, S.; Baccile, N.; De Maeseneire, S.L.; Roelants, S.L.K.W.; Soetaert, W.K. From bumblebee to bioeconomy: Recent developments and perspectives for sophorolipid biosynthesis. *Biotechnol. Adv.* **2021**, 107788. [[CrossRef](#)] [[PubMed](#)]
5. Develter, D.W.G.; Laurysen, L.M.L. Properties and industrial applications of sophorolipids. *Eur. J. Lipid Sci. Technol.* **2010**, *112*, 628–638. [[CrossRef](#)]
6. Hirata, Y.; Ryu, M.; Igarashi, K.; Nagatsuka, A.; Furuta, T.; Kanaya, S.; Sugiura, M. Natural synergism of acid and lactone type mixed sophorolipids in interfacial activities and cytotoxicities. *J. Oleo Sci.* **2009**, *58*, 565–572. [[CrossRef](#)]
7. Kasture, M.; Singh, S.; Patel, P.; Joy, P.A.; Prabhune, A.A.; Ramana, C.V.; Prasad, B.L.V. Multiutility sophorolipids as nanoparticle capping agents: Synthesis of stable and water dispersible Co nanoparticles. *Langmuir* **2007**, *23*, 11409–11412. [[CrossRef](#)]
8. Nguyen, T.T.; Sabatini, D.A. Characterization and emulsification properties of rhamnolipid and sophorolipid biosurfactants and their applications. *Int. J. Mol. Sci.* **2011**, *12*, 1232–1244. [[CrossRef](#)]
9. Van Renterghem, L.; Roelants, S.L.K.W.; Baccile, N.; Uyttersprot, K.; Taelman, M.C.; Everaert, B.; Mincke, S.; Ledegen, S.; Debrouwer, S.; Scholtens, K.; et al. From lab to market: An integrated bioprocess design approach for new-to-nature biosurfactants produced by *Starmerella bombicola*. *Biotechnol. Bioeng.* **2018**, *115*, 1195–1206. [[CrossRef](#)]
10. Van Bogaert, I.N.A.; Saerens, K.; De Muyck, C.; Develter, D.; Soetaert, W.; Vandamme, E.J. Microbial production and application of sophorolipids. *Appl. Microbiol. Biotechnol.* **2007**, *76*, 23–34. [[CrossRef](#)]
11. Kim, K.; Dalsoo, Y.; Youngbum, K.; Baekseok, L.; Doonhoon, S.; Eun-Ki, K. Characteristics of sophorolipid as an antimicrobial agent. *J. Microbiol. Biotechnol.* **2002**, *12*, 235–241.
12. Delbeke, E.I.P.; Roelants, S.L.K.W.; Matthijs, N.; Everaert, B.; Soetaert, W.; Coenye, T.; Van Geem, K.M.; Stevens, C.V. Sophorolipid Amine Oxide Production by a Combination of Fermentation Scale-up and Chemical Modification. *Ind. Eng. Chem. Res.* **2016**, *55*, 7273–7281. [[CrossRef](#)]
13. Zhang, L.; Somasundaran, P.; Singh, S.K.; Felse, A.P.; Gross, R. Synthesis and interfacial properties of sophorolipid derivatives. *Colloids Surfaces A Physicochem. Eng. Asp.* **2004**, *240*, 75–82. [[CrossRef](#)]
14. Israelachvili, J.N.; Mitchell, D.J.; Ninham, B.W. Theory of self-assembly of hydrocarbon amphiphiles into micelles and bilayers. *J. Chem. Soc. Faraday Trans. Mol. Chem. Phys.* **1976**, *72*, 1525–1568. [[CrossRef](#)]
15. Baccile, N.; Seyrig, C.; Poirier, A.; Alonso-de Castro, S.; Roelants, S.L.K.W.; Abel, S. Self-assembly, interfacial properties, interactions with macromolecules and molecular modelling and simulation of microbial bio-based amphiphiles (biosurfactants). A tutorial review. *Green Chem.* **2021**, *23*, 3842–3944. [[CrossRef](#)]
16. Baccile, N.; Cuvier, A.-S.; Prévost, S.; Stevens, C.V.; Delbeke, E.; Berton, J.; Soetaert, W.; Van Bogaert, I.N.A.; Roelants, S. Self-Assembly Mechanism of pH-Responsive Glycolipids: Micelles, Fibers, Vesicles, and Bilayers. *Langmuir* **2016**, *32*, 10881–10894. [[CrossRef](#)]
17. Baccile, N.; Babonneau, F.; Jestin, J.; Pehau-Arnaudet, G.; Van Bogaert, I. Unusual, pH-induced, self-assembly of sophorolipid biosurfactants. *ACS Nano* **2012**, *6*, 4763–4776. [[CrossRef](#)]
18. Shrestha, R.G.; Shrestha, L.K.; Aramaki, K. Rheology of wormlike micelles in aqueous systems of a mixed amino acid-based anionic surfactant and cationic surfactant. *Colloid Polym. Sci.* **2009**, *287*, 1305–1315. [[CrossRef](#)]
19. Chen, M.L.; Penfold, J.; Thomas, R.K.; Smyth, T.J.P.; Perfumo, A.; Marchant, R.; Banat, I.M.; Stevenson, P.; Parry, A.; Tucker, I.; et al. Solution self-assembly and adsorption at the air-water interface of the monorhamnolipid and dirhamnolipid rhamnolipids and their mixtures. *Langmuir* **2010**, *26*, 18281–18292. [[CrossRef](#)]
20. Ishigami, Y.; Gama, Y.; Nagahora, H.; Yamaguchi, M.; Nakahara, H.; Kamata, T. The pH-Sensitive Conversion of Molecular Aggregates of Rhamnolipid Biosurfactant. *Chem. Lett.* **1987**, *16*, 763–766. [[CrossRef](#)]

21. Champion, J.T.; Gilkey, J.C.; Lamparski, H.; Retterer, J.; Miller, R.M. Electron microscopy of rhamnolipid (biosurfactant) morphology: Effects of pH, cadmium, and octadecane. *J. Colloid Interface Sci.* **1995**, *170*, 569–574. [[CrossRef](#)]
22. Xu, L.; Amin, S. Microrheological study of ternary surfactant-biosurfactant mixtures. *Int. J. Cosmet. Sci.* **2019**, *41*, 364–370. [[CrossRef](#)] [[PubMed](#)]
23. Kleinen, J.; Venzmer, J. Streaming potential measurements to understand the rheological properties of surfactant formulations containing anionic and zwitterionic surfactant. *J. Cosmet. Sci.* **2016**, *67*, 59–70. [[PubMed](#)]
24. Patist, A.; Oh, S.G.; Leung, R.; Shah, D.O. Kinetics of micellization: Its significance to technological processes. *Colloids Surfaces A Physicochem. Eng. Asp.* **2001**, *176*, 3–16. [[CrossRef](#)]
25. Cates, M.E. Nonlinear viscoelasticity of wormlike micelles (and other reversibly breakable polymers). *J. Phys. Chem.* **1990**, *94*, 371–375. [[CrossRef](#)]
26. Schroyen, B.; Vlassopoulos, D.; Van Puyvelde, P.; Vermant, J. Bulk rheometry at high frequencies: A review of experimental approaches. *Rheol. Acta* **2020**, *59*, 1–22. [[CrossRef](#)]
27. Zou, W.; Tan, G.; Jiang, H.; Vogtt, K.; Weaver, M.; Koenig, P.; Beaucage, G.; Larson, R.G. From well-entangled to partially-entangled wormlike micelles. *Soft Matter* **2019**, *15*, 642–655. [[CrossRef](#)]
28. Amin, S.; Blake, S.; Kennel, R.; Lewis, E. Revealing New Structural Insights from Surfactant Micelles through DLS, Microrheology and Raman Spectroscopy. *Materials* **2015**, *8*, 3754–3766. [[CrossRef](#)]
29. Dasgupta, B.R.; Weitz, D.A. Microrheology of cross-linked polyacrylamide networks. *Phys. Rev. E-Stat. Nonlinear Soft Matter Phys.* **2005**, *71*, 1–9. [[CrossRef](#)]
30. Krajina, B.A.; Tropini, C.; Zhu, A.; DiGiacomo, P.; Sonnenburg, J.L.; Heilshorn, S.C.; Spakowitz, A.J. Dynamic Light Scattering Microrheology Reveals Multiscale Viscoelasticity of Polymer Gels and Precious Biological Materials. *ACS Cent. Sci.* **2017**, *3*, 1294–1303. [[CrossRef](#)]
31. Cai, P.C.; Krajina, B.A.; Kratochvil, M.J.; Zou, L.; Zhu, A.; Burgener, E.B.; Bollyky, P.L.; Milla, C.E.; Webber, M.J.; Spakowitz, A.J.; et al. Dynamic light scattering microrheology for soft and living materials. *Soft Matter* **2021**, *17*, 1929–1939. [[CrossRef](#)]
32. Amin, S.; Rega, C.A.; Jankevics, H. Detection of viscoelasticity in aggregating dilute protein solutions through dynamic light scattering-based optical microrheology. *Rheol. Acta* **2012**, *51*, 329–342. [[CrossRef](#)]
33. Baccile, N.; Van Renterghem, L.; Le Griel, P.; Ducouret, G.; Brennich, M.; Cristiglio, V.; Roelants, S.L.K.W.; Soetaert, W. Bio-based glyco-bolaamphiphile forms a temperature-responsive hydrogel with tunable elastic properties. *Soft Matter* **2018**, *14*, 7859–7872. [[CrossRef](#)]
34. Mason, T.G.; Weitz, D.A. Optical Measurements of Frequency-Dependent Linear Viscoelastic Moduli of Complex Fluids. *Phys. Rev. Lett.* **1995**, *74*, 1250–1253. [[CrossRef](#)] [[PubMed](#)]
35. Microrheology Feature Key. Available online: <https://www.malvernstore.com/en-gb/categories/software/cps0125> (accessed on 8 October 2021).
36. Willenbacher, N.; Oelschlaeger, C.; Schopferer, M.; Fischer, P.; Cardinaux, F.; Scheffold, F. Broad bandwidth optical and mechanical rheometry of wormlike micelle solutions. *Phys. Rev. Lett.* **2007**, *99*, 68302. [[CrossRef](#)] [[PubMed](#)]
37. Oelschlaeger, C.; Willenbacher, N. Mixed wormlike micelles of cationic surfactants: Effect of the cosurfactant chain length on the bending elasticity and rheological properties. *Colloids Surfaces A Physicochem. Eng. Asp.* **2012**, *406*, 31–37. [[CrossRef](#)]
38. Bharadwaj, N.A.; Ewoldt, R.H. Single-point parallel disk correction for asymptotically nonlinear oscillatory shear. *Rheol. Acta* **2015**, *54*, 223–233. [[CrossRef](#)]
39. Costello, B. The AR-G2 Magnetic Bearing Rheometer. 2005. Available online: [http://www.tainstruments.com/pdf/literature/RH085\\_AR\\_G2\\_performance.pdf](http://www.tainstruments.com/pdf/literature/RH085_AR_G2_performance.pdf) (accessed on 25 November 2021).
40. Cox, W.P.; Merz, E.H. Correlation of dynamic and steady flow viscosities. *J. Polym. Sci.* **1958**, *28*, 619–622. [[CrossRef](#)]
41. Zhou, S.; Xu, C.; Wang, J.; Gao, W.; Akhverdijeva, R.; Shah, V.; Gross, R. Supramolecular assemblies of a naturally derived sophorolipid. *Langmuir* **2004**, *20*, 7926–7932. [[CrossRef](#)]
42. Hirata, Y.; Ryu, M.; Ito, H.; Araki, M. Saraya Co. Ltd. High-Purity Acid-Form Sophorolipid (SL) Containing Composition and Process for Preparing Same. European Patent EP2821495A1, 7 January 2015.
43. Agrawal, N.R.; Yue, X.; Raghavan, S.R. The Unusual Rheology of Wormlike Micelles in Glycerol: Comparable Timescales for Chain Reptation and Segmental Relaxation. *Langmuir* **2020**, *36*, 6370–6377. [[CrossRef](#)]
44. Cardinaux, F.; Cipelletti, L.; Scheffold, F.; Schurtenberger, P. Microrheology of giant-micelle solutions. *Europhys. Lett.* **2002**, *57*, 738–744. [[CrossRef](#)]
45. Luger, J.; Stettin, H. Effects of instrument and fluid inertia in oscillatory shear in rotational rheometers. *J. Rheol.* **2016**, *60*, 393–406. [[CrossRef](#)]
46. Dhasaiyan, P.; Le Griel, P.; Roelants, S.; Redant, E.; Van Bogaert, I.N.A.; Prevost, S.; Prasad, B.L.V.; Baccile, N. Micelles versus Ribbons: How Congeners Drive the Self-Assembly of Acidic Sophorolipid Biosurfactants. *ChemPhysChem* **2017**, *18*, 643–652. [[CrossRef](#)] [[PubMed](#)]
47. Baccile, N.; Pedersen, J.S.; Pehau-Arnaudet, G.; Van Bogaert, I.N.A. Surface charge of acidic sophorolipid micelles: Effect of base and time. *Soft Matter* **2013**, *9*, 4911–4922. [[CrossRef](#)]
48. Hayward, D.W.; Chiappisi, L.; Teo, J.H.; Prevost, S.; Schweins, R.; Gradzielski, M. Neutralisation rate controls the self-assembly of pH-sensitive surfactants. *Soft Matter* **2019**, *15*, 8611–8620. [[CrossRef](#)] [[PubMed](#)]